vehicles

MDPI

Article

Thermal-Based Driver Monitoring in an Automotive Environment Using a Mobile Camera: A Feasibility Study

Yordan Stoyanov [1,2]

[1] Department of Transport and Aircraft Equipment and Technologies, Technical University of Sofia, Branch Plovdiv, 25 Tsanko Dyustabanov Street, 4000 Plovdiv, Bulgaria; yordan.stoyanov@tu-plovdiv.bg
[2] Center of Competence "Smart Mechatronic, Eco-and Energy-Saving Systems and Technologies", Technical University of Sofia, Branch Plovdiv, 4000 Plovdiv, Bulgaria

Abstract

This study evaluates the feasibility, repeatability, and temporal consistency of a low-cost long-wave infrared (LWIR) thermal imaging workflow for in-vehicle driver monitoring under realistic operating conditions. Two participants were monitored during three independent 60 min driving sessions each. Facial thermal observations were obtained using a consumer-grade mobile LWIR camera operated through a smartphone application environment. Forehead-region temperature data were extracted from a manually positioned region of interest (ROI), including center-point, mean, maximum, and minimum temperature values. Geometric validation was first performed under stationary vehicle conditions in order to confirm forehead-ROI visibility and stability across multiple head orientations and posture variations. Subsequent dynamic sessions were used to evaluate cross-session repeatability and temporal behavior of sampled ROI-based thermal metrics. The results show that the facial thermal patterns remained structurally consistent across repeated sessions, while the sampled temperature trajectories exhibited generally smooth behavior without evidence of progressive within-session instability over the 60 min recordings. Although minor inter-session offsets were observed, normalized analysis confirmed preservation of the relative temporal dynamics. The findings indicate that the examined low-cost LWIR workflow can provide sufficiently stable and repeatable facial thermal observations for feasibility-level driver monitoring analysis under realistic in-vehicle conditions. The contribution of this work lies in a structured validation methodology combining geometric validation, cross-session repeatability, and temporal consistency assessment as a methodological foundation for future thermal-based driver monitoring applications.

Keywords: thermal imaging; driver monitoring; long-wave infrared; LWIR; mobile thermal camera; ROI-based temperature analysis; temporal consistency; cross-session repeatability; in-vehicle monitoring

Check for updates

Academic Editor: Mohammed Chadli

Received: 18 February 2026
Revised: 22 April 2026
Accepted: 25 May 2026
Published: 27 May 2026

Correction Statement: This article has been republished with a minor change. The change does not affect the scientific content of the article and further details are available within the backmatter of the website version of this article.

Copyright: © 2026 by the author. Licensee MDPI, Basel, Switzerland. This article is an open access article distributed under the terms and conditions of the Creative Commons Attribution (CC BY) license.

1. Introduction

Driver monitoring has become an essential component of modern automotive safety systems due to the need to reduce accidents associated with fatigue, distraction, and reduced vigilance. Among the available driver-state indicators, head pose, head motion, gaze behavior, and facial activity are particularly informative, since changes in posture, visual attention, and corrective movements may precede a clear decline in alertness or performance. Consequently, driver monitoring has been extensively studied using visible-spectrum imaging, geometric head-tracking methods, optical flow-based motion analysis, and model-based facial tracking approaches [1–6].

Classical vision-based approaches demonstrated promising performance under controlled conditions, including elliptical head tracking, motion-regularized face tracking, three-dimensional head pose estimation, and camera-based monitoring of head and eye motion [2–6]. More recent studies have extended this direction toward real-time embedded systems, driver activity recognition, multi-task fusion algorithms, and deep learning-based monitoring of gaze, eyes, mouth, and head position [7–13]. In addition to camera-only systems, other driver monitoring solutions have included orientation sensors and multimodal sensing strategies for tracking driver behavior and driver state [13,14]. However, despite substantial progress, visible-spectrum systems remain inherently sensitive to illumination variability, shadows, reflections, and rapid lighting transitions, which are unavoidable in real automotive environments. Even during daytime driving, sunlight angle, roadside occlusions, and cabin reflections can reduce robustness, while night-time operation introduces further limitations due to poor illumination and glare.

To address these limitations, alternative non-visible sensing modalities have been explored. Near-infrared (NIR) systems have been used for gaze detection, eye localization, and contactless in-vehicle vital sign monitoring, showing that non-visible sensing can improve robustness under challenging lighting conditions [10,11]. Long-wave infrared (LWIR) thermal imaging represents another important alternative because it captures emitted thermal radiation rather than reflected visible light. As a result, thermal imaging is inherently less dependent on ambient illumination and can remain informative during both day and night operation. Beyond geometric visibility, thermal imagery can also provide surface temperature-related information linked to physiological processes such as blood perfusion, respiration, stress, workload, and thermoregulation, making this modality relevant to driver state monitoring [15–24].

Several previous studies have investigated thermal imaging approaches in relation to driver monitoring, including respiration monitoring, facial temperature variation, thermal correlates of drowsiness, and infrared-based assessment of driver workload [16–24]. Thermal facial features have been used in simulator-based drowsiness studies, while more recent work has combined thermal imagery with machine learning for driver vigilance or workload classification [17–23]. At the same time, research on forehead skin temperature has shown that thermal variations may accompany changes in alertness and physiological condition [21]. These findings support the broader relevance of thermal facial observation for driver state-related applications. However, such studies do not necessarily constitute direct validation of a deployable driver monitoring workflow under real in-vehicle conditions, especially when low-cost consumer-grade devices are considered.

Despite its advantages, facial observation and tracking in the LWIR domain remain challenging. Compared with visible-light images, thermal images typically exhibit lower spatial resolution, reduced texture detail, and limited contrast between adjacent regions due to relatively small temperature gradients. As a result, feature descriptors and tracking algorithms originally developed for visible imagery, such as scale-invariant feature transform (SIFT), may perform less reliably when applied directly to thermal data [25]. In addition, consumer-grade mobile thermal cameras often operate through smartphone-based application environments, provide displayed temperature information rather than raw radiometric export, and impose practical constraints on reproducibility, post-processing, and (ROI) definition. These limitations are particularly important when the goal is not simply qualitative observation but stable frame-based analysis under realistic driving conditions.

In parallel with the sensing modality itself, the in-vehicle thermal environment also affects driver comfort and alertness. Cabin temperature, airflow, and thermal microclimate can influence skin temperature and thermoregulation, which may in turn affect the interpretation of facial thermal measurements. This means that thermal observations obtained

in a vehicle cabin should be evaluated not only from the perspective of sensor visibility but also with regard to environmental consistency and repeatability across sessions.

Against this background, the present study evaluates whether a compact consumer-grade mobile LWIR camera can provide sufficiently stable and repeatable facial thermal observations in a real automotive cabin. The focus is placed on geometric visibility, cross-session repeatability, and temporal consistency of a manually assisted forehead-ROI workflow. As a prerequisite for future driver state inference, the present work is intentionally limited to signal-level feasibility validation rather than behavioral or drowsiness-specific analysis. The contribution of this study lies in its structured assessment of whether an app-based low-cost LWIR workflow can preserve adequate facial thermal consistency for ROI-based monitoring under realistic in-vehicle conditions.

2. Materials and Methods

To avoid over-interpretation, the present work was positioned as a feasibility-level investigation focused on sensor deployment, data stability, and quantitative thermal observation under real driving conditions, rather than as a validated drowsiness classification study.

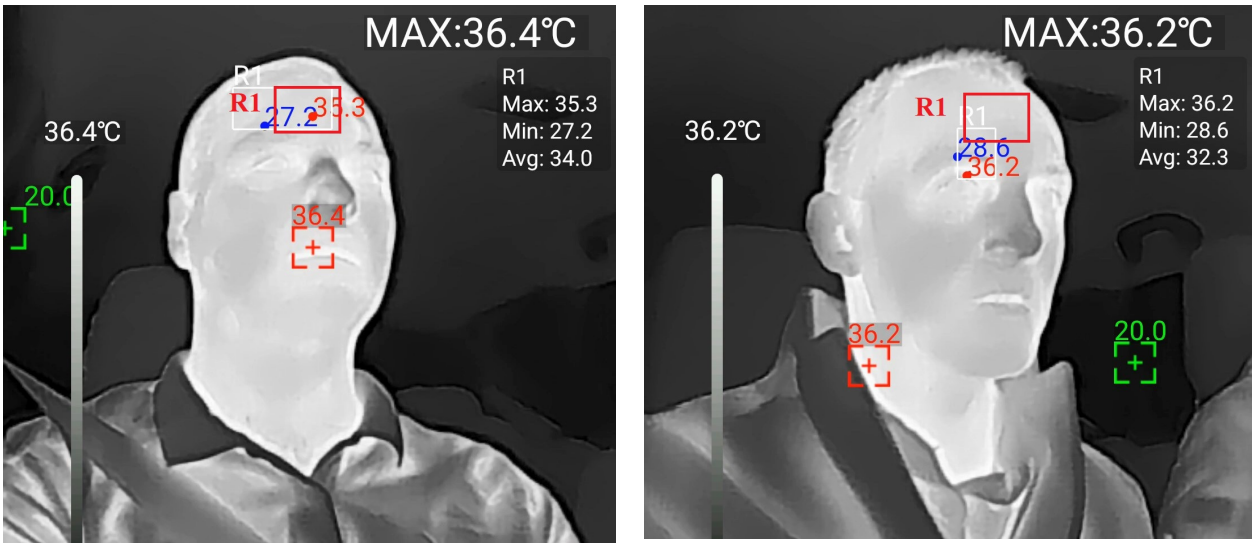
2.1. Experimental Setup

The experimental study was conducted in a passenger vehicle under real-world driving conditions. Prior to data acquisition, the cabin air temperature was stabilized in order to ensure thermal comfort and to reduce variability in the driver's infrared signature caused by transient environmental changes. This procedure was intended to minimize external thermal influences and improve the consistency of thermal observations across sessions.

The experimental campaign consisted of six driving sessions, each with a fixed duration of 60 min, conducted on separate days under comparable real-world driving conditions. All sessions were performed in the morning and followed similar routes characterized by relatively steady traffic flow and limited external disturbances. Driving speed varied between 60 and 90 km/h throughout each 60 min session. Two adult participants were included in this study. Participant I was a 39-year-old male, and Participant II was a 37-year-old male. Both participants were healthy and reported no acute illness over the measurement period.

Thermal video of the driver was recorded using a compact handheld long-wave infrared (LWIR) thermal camera (UTi260M by Uni-Trend Technology Co., Ltd. Located in Dongguan City, China. The camera was operated using the UNI—T Thermal Mobile smartphone application). The camera was positioned so as to maintain a clear and consistent field of view of the driver's head and upper torso throughout the driving session without interfering with normal driving behavior. The camera field of view was defined by a cone with an apex angle of 56°. Orientation and distance were kept fixed to minimize geometric variation in the recorded thermal patterns. The camera mounting configuration inside the vehicle cabin is illustrated in Figure 1.

The driving task was performed on a long, uniform road segment selected to induce relatively monotonous driving conditions. This choice was made in order to ensure extended steady-state driving exposure under comparable operational constraints. Thermal video data were acquired continuously during each session at a frame rate of 25 Hz through the smartphone application environment.



(**a**) (**b**)

Figure 1. Representative thermal frames showing manual placement of the forehead ROI (R1) used for extraction of center-point, mean, maximum, and minimum temperature values: (**a**) Participant I; (**b**) Participant II.

2.2. Thermal Imaging Device

The UTi260M is a mobile LWIR thermal imaging module designed for smartphone-based operation. It employs an uncooled vanadium oxide microbolometer detector with a spatial resolution of 256 × 192 pixels and a spectral response in the 8–14 µm wavelength range. The device supports temperature measurements from −20 °C to 550 °C and provides enhanced accuracy in the human body temperature range, shown in Table 1.

Table 1. UTi260M thermal imager specifications.

Sensor	Uncooled Vanadium Oxide
Range switching	Low temperature (−20–150 °C), high temperature (0–550 °C) (auto switching)
Modes	Industrial, human body
Emissivity	0.95 (default) 0.01–1.00
IR resolution	256 × 192 (49,152)
Infrared spectral bandwidth	8–14 µm
Thermal sensitivity	<50 mK
Frame rate	25 Hz

Thermal images are displayed using selectable color palettes and include real-time temperature mapping, point and area measurements, and automatic tracking of maximum and minimum temperature values. Due to its compact size and consumer-grade design, the device represents a cost-effective alternative to industrial thermal cameras commonly used in automotive research.

2.3. Data Acquisition and Preprocessing

The UTi260M camera was used through its smartphone-based application environment, which provided thermal image visualization and surface temperature display functions but did not provide access to raw detector-level radiometric data for the present workflow. Accordingly, the present study was based on app-displayed thermal imagery and manually positioned temperature windows rather than on native radiometric frame export.

Thermal observations were processed offline using a sampled-frame feasibility workflow rather than exhaustive frame-by-frame annotation of the entire 25 Hz dataset. Single

representative frames were extracted at 5 min intervals from each 60 min session, yielding 12 sampled analysis frames per session and 72 sampled frames in total across all six sessions.

For each selected frame, the forehead temperature window was positioned manually for the corresponding driver in the upper frontal facial region above the periorbital area and below the hairline, while avoiding obvious background inclusion and peripheral non-target regions. This manual placement was used deliberately in order to avoid losing the target forehead zone in low-resolution LWIR imagery. ROI placement was performed by a single operator throughout the dataset in order to maintain internal consistency of the manually assisted workflow.

Representative thermal frames showing manual placement of the forehead ROI (R1) used for ROI-based extraction are provided in Figure 1.

The key specifications of the thermal imager are summarized in Table 1, while the physical configuration and camera placement within the vehicle are illustrated in Figures 2 and 3.



Figure 2. UTi260M thermal imager.

Natural vehicle vibration and subtle head micro-movements were present during real driving. To reduce obvious motion-related artifacts in the quantitative feasibility-level analysis, only frames with visually stable facial capture and clearly preserved forehead-region visibility were selected.

Because raw radiometric detector data were not available, frame-based temperature interpretation was limited to the thermal information displayed by the smartphone application. Therefore, the reported temperature-derived values should be interpreted as approximate workflow-level measurements rather than as fully validated detector-level radiometric data.

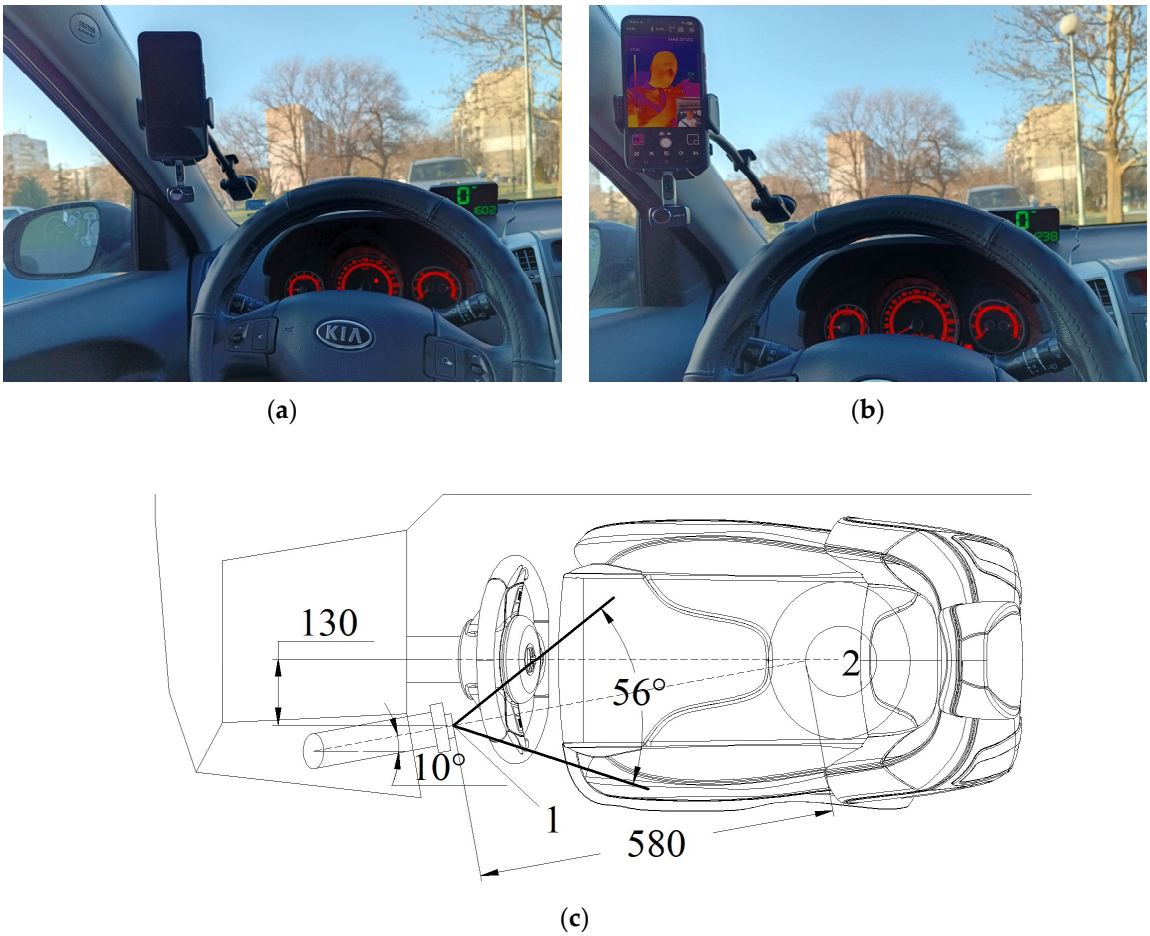


Figure 3. Thermal camera position (**a**,**b**) in automotive environment; (**c**) thermal camera positions: 1—thermal camera, 2—human body.

2.4. Analysis Strategy

The analysis focused on evaluating thermal signal stability, ROI-based temperature consistency, and cross-session repeatability under repeated real-driving sessions. Observable posture changes were considered only qualitatively as contextual observations and were not quantified in the present study.

The quantitative analysis was based on sampled ROI-derived temperature metrics, including center-point, mean, maximum, and minimum values within the forehead temperature window. In addition, within-session stability was assessed using the ROI mean slope and coefficient of variation, whereas inter-session comparison was evaluated using Pearson correlation and root mean square error (RMSE) of the mean ROI trajectories.

Rather than implementing automated classification or detection algorithms, this study adopted a feasibility-oriented approach. The objective was to evaluate whether a consumer-grade mobile LWIR camera could deliver sufficiently stable thermal observations to support future development of non-contact driver monitoring and alerting systems under real driving conditions.

2.5. Frame-Based Thermal Consistency Assessment

Because the camera workflow used in the present study did not provide raw detector-level radiometric frame export, the analysis was limited to app-displayed thermal imagery and manually positioned temperature windows. Accordingly, the assessment focused on practical frame-level consistency of the thermal facial representation, preservation of the

forehead-region thermal pattern, and repeatability of sampled ROI-based temperature observations across sessions.

A pixel-wise temperature interpretation was derived from the displayed thermal image and its associated color scale when required for ROI-based analysis. In this context, the extracted temperature-related values should be interpreted as approximate workflow-level measures rather than strict detector-calibration quantities.

This quantitative framework was intentionally selected to evaluate feasibility-level thermal repeatability and temporal consistency under a practical app-based consumer imaging workflow without relying on unsupported detector-level calibration assumptions.

3. Results

3.1. Workflow-Level Thermal Frame Consistency

Table 2 summarizes the sampled-frame thermal analysis workflow used in the present study. Because the UTi260M camera was operated through its smartphone application environment and did not provide raw detector-level radiometric frame export, the present analysis was intentionally limited to workflow-level thermal frame consistency rather than strict detector-calibration metrics.

Table 2. Summary of the sampled-frame thermal analysis workflow used in the present study.

Parameter	Value
Continuous thermal video acquisition rate	25 Hz
Duration of each driving session	60 min
Number of driving sessions	6
Number of participants	2
Temporal sampling interval for quantitative analysis	5 min
Sampled frames per session	12
Total sampled frames analyzed	72
Thermal data source	Smartphone application displayed thermal imagery
Raw detector-level radiometric export	Not available
ROI handling	Manually positioned forehead temperature window
Frame inclusion criterion	Visually stable facial capture with clearly preserved forehead-region visibility

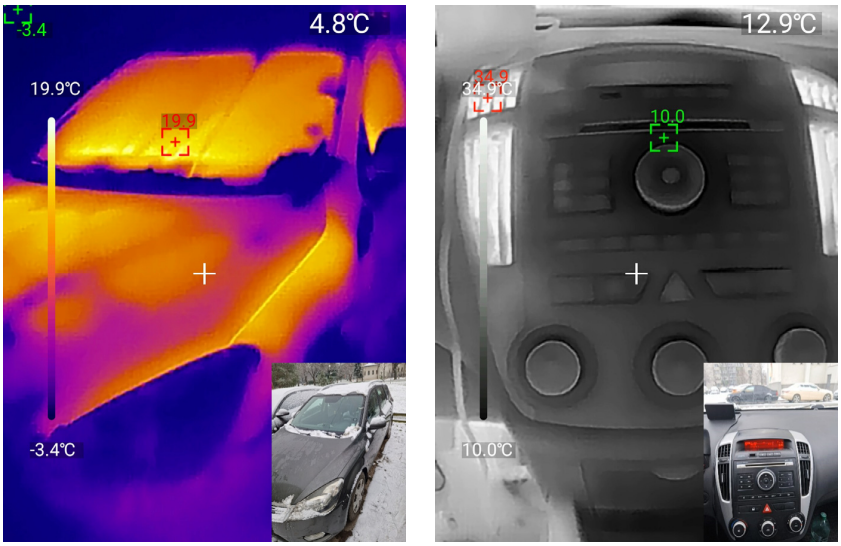
The app-displayed thermal frames provided sufficiently stable facial visibility and preserved forehead-region thermal representation to support manually assisted ROI placement, cross-session frame comparison, and the sampled temporal analyses reported in the following sections. Accordingly, this study focuses on feasibility-level consistency of the practical mobile thermal imaging workflow rather than on full radiometric sensor characterization.

3.2. Environmental and Session Control Conditions

All driving sessions were conducted under controlled and comparable environmental conditions. A total of six sessions (S1–S6) were performed in the morning hours, each with a duration of 60 min. None of the sessions were conducted after a workday, thereby helping to maintain comparable baseline conditions across recordings.

The environmental boundary conditions were documented using thermal imaging of both the external vehicle surface and the interior cabin. Representative images are shown in Figure 4. During the experimental sessions, the outdoor temperature ranged between −1 °C and 0 °C, while the cabin temperature was stabilized at approximately 23 °C.

A summary of contextual and environmental parameters is provided in Table 3. The documented thermal gradient between exterior winter conditions and the stabilized cabin environment confirms that the measurements were obtained under controlled and reproducible thermal conditions.



(**a**) (**b**)

Figure 4. Optimal heat exchange in the vehicle: (**a**) outside of the vehicle; (**b**) outside of the vehicle.

Table 3. Summary of driving sessions, including contextual parameters and environmenta conditions.

Session ID	Time of Day	After Workday, Yes/No	Duration, min	Cabin Temp., °C	Outside Temp., °C
S1	Morning	No	60	23	−1
S2	Morning	No	60	23	−1
S3	Morning	No	60	23	−1
S4	Morning	No	60	23	0
S5	Morning	No	60	23	0
S6	Morning	No	60	23	0

Representative RGB frontal frames for Participant I and Participant II are shown in Figure 5. These images were acquired using the same mobile device in visible-spectrum mode with the thermal sensor disabled. This figure illustrates the frontal head geometry, facial proportions, and baseline posture under identical camera placement and cabin conditions. This RGB modality serves as a geometric reference for subsequent cross-modal comparison with the LWIR recordings.



(**a**) (**b**)

Figure 5. Frontal RGB reference images of Participant I and Participant II acquired using the same mobile device with the thermal sensor disabled. The images illustrate baseline head geometry and

camera alignment under identical in-vehicle mounting conditions. These frames serve as visible-spectrum reference data for subsequent cross-modal geometric validation with LWIR recordings: (**a**) Participant I; (**b**) Participant II.

Together, these observations establish a geometric and environmental baseline for the subsequent thermal consistency analysis.

3.3. Controlled Pose Sequences—Participant I

Figure 6 presents synchronized RGB (top row) and LWIR (bottom row) frames for Participant I under controlled stationary conditions. Each RGB image is paired with the corresponding thermal frame acquired at the same time point. Subfigure pairs (a–e), (b–f), (c–g), and (d–h) represent corresponding head configurations recorded simultaneously in visible and thermal modalities.

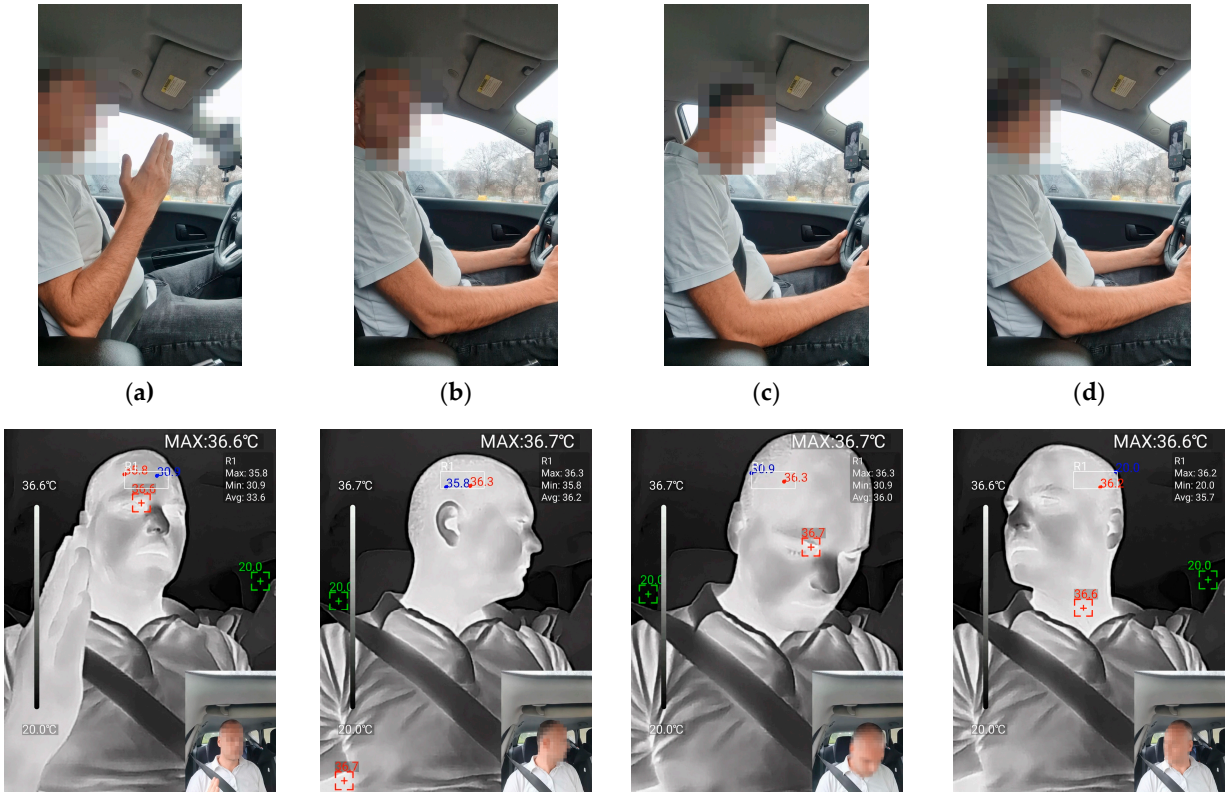
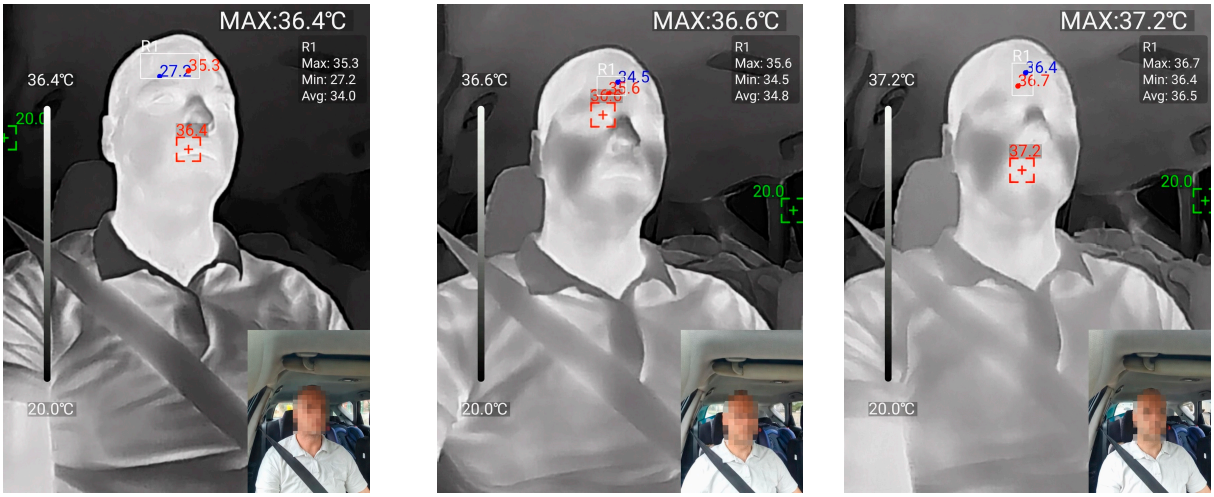


Figure 6. Controlled head pose sequence for Participant I under stationary vehicle conditions. The top row (**a**–**d**) shows RGB frames acquired in visible-spectrum mode, while the bottom row (**e**–**h**) presents the corresponding synchronized LWIR frames. Subfigure pairs (**a**–**e**), (**b**–**f**), (**c**–**g**), and (**d**–**h**) represent identical head configurations captured simultaneously in both modalities. The sequence includes neutral, yaw, and pitch poses, demonstrating geometric consistency between RGB reference images and thermal centroid displacement.

The sequence includes neutral posture, lateral yaw rotations, and downward pitch inclination. The RGB frames provide a geometric reference view, while the LWIR frames show consistent thermal facial representation and corresponding centroid displacement. The visual correspondence between paired subfigures confirms cross-modal geometric coherence under stationary vehicle conditions.

3.4. Mid-Session Thermal Stability—Participant I

Figure 7 presents representative LWIR frames of Participant I acquired at the midpoint of each of the three driving sessions. The images were extracted at comparable time points to evaluate thermal consistency under similar cabin conditions.



(**a**) (**b**) (**c**)

Figure 7. Representative LWIR frames of Participant I acquired at the midpoint of three separate driving sessions: (**a**) Session 1; (**b**) Session 2; (**c**) Session 3. Each image corresponds to a different recording day under comparable cabin conditions. Despite minor variations in maximum temperature values, the overall facial thermal distribution and spatial gradients remain consistent, demonstrating the temporal stability and repeatability of the LWIR system.

Despite minor variations in maximum recorded temperature values (36.4 °C, 36.6 °C, and 37.2 °C), the spatial facial temperature distribution remains consistent across sessions. The relative thermal gradients between the forehead, nasal region, and background surfaces are preserved.

The uniform appearance of facial contours and the absence of obvious structural artifacts indicate stable thermal representation across separate recording days.

These observations support the repeatability of the LWIR workflow under repeated real-vehicle deployment conditions.

3.5. Mid-Session Thermal Stability—Participant II

Figure 8 presents representative LWIR frames of Participant II extracted at the midpoint of each of the three independent driving sessions. The images were selected at comparable time points to assess cross-session repeatability of facial thermal distribution.

The maximum recorded temperatures across sessions (36.2 °C, 36.4 °C, and 37.1 °C) show minor variation, while the spatial distribution of the facial thermal gradients remains structurally consistent. The forehead, nasal, and periorbital regions exhibit stable relative intensity patterns.

No abrupt structural artifacts or contour distortions are visible in the selected frames. The preserved facial contours across recording days indicate repeatable thermal representation under comparable in-vehicle conditions.

The comparable cross-session stability observed for both participants in Figures 7 and 8 supports the repeatability of the mobile LWIR workflow under repeated real-world deployment conditions.



(**a**) (**b**) (**c**)

Figure 8. Representative LWIR frames of Participant II acquired at the midpoint of three separate driving sessions: (**a**) Session 1; (**b**) Session 2; (**c**) Session 3. Each image corresponds to a different recording day under similar cabin conditions. Despite minor variation in maximum temperature values, the overall facial thermal gradients and spatial distribution remain consistent, demonstrating the repeatability and temporal stability of the LWIR deployment.

3.6. Temporal Thermal Evolution—Participant I

Figure 9 presents the temporal evolution of selected thermal metrics for Participant I across three independent driving sessions. The analyzed parameters include center-point temperature, mean forehead temperature within the defined ROI, maximum forehead temperature, and minimum forehead temperature. The reported time series were generated from single sampled frames extracted at 5 min intervals from the continuous 25 Hz recordings.

Across all sessions, the center-point temperature (Figure 9a), central point, remains within a relatively narrow range, with gradual fluctuations over the 60 min duration. No abrupt temperature discontinuities or progressive drift behavior are observed.

The mean forehead temperature (Figure 9b) (ROI) shows moderate temporal variation. Session 2 includes an isolated decrease between approximately 20 and 30 min. Given the manually positioned ROI workflow, sampled-frame analysis, and display-based temperature interpretation, this event is interpreted conservatively as a likely frame-level measurement anomaly related to ROI sensitivity or partial peripheral inclusion rather than as robust evidence of a physiological forehead temperature decrease of such magnitude.

The maximum forehead temperature values (Figure 9c), forehead max, follow trends consistent with the center-point measurements, indicating stable upper-bound thermal response across sessions. The minimum forehead temperature values (Figure 9d), forehead min, show greater variability than the mean and maximum ROI metrics. This is expected because the minimum value is particularly sensitive to localized cooling, small ROI boundary shifts, and intermittent inclusion of cooler peripheral pixels. Although frames with obvious motion artifacts were excluded during manual selection, minor residual effects related to natural driving vibration and subtle facial micro-movements may still have contributed to the increased variability of the minimum-temperature signal.

To facilitate inter-session comparison, the normalized forehead temperature trends are shown in Figure 10. Normalization reduces absolute offsets and highlights relative temporal dynamics. The general progression across sessions demonstrates comparable trend behavior without structural divergence.

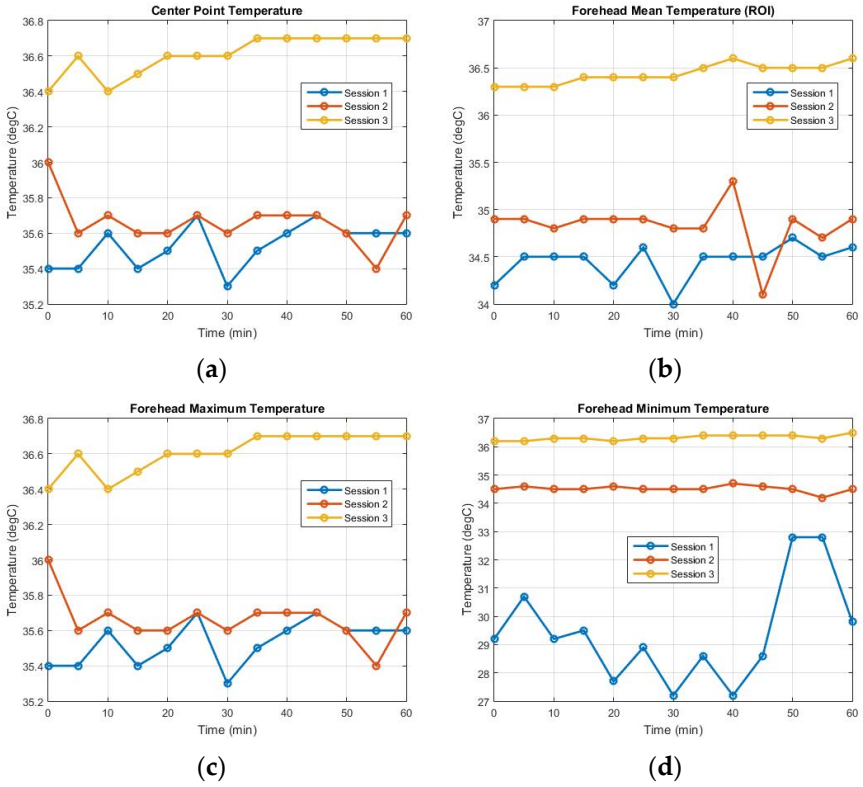


Figure 9. Temporal thermal metrics for Participant I across three independent driving sessions. (**a**) Center-point temperature, (**b**) mean forehead temperature within the ROI, (**c**) maximum forehead temperature, and (**d**) minimum forehead temperature. The 60 min time series demonstrates stable sensor behavior and absence of structural drift across sessions.

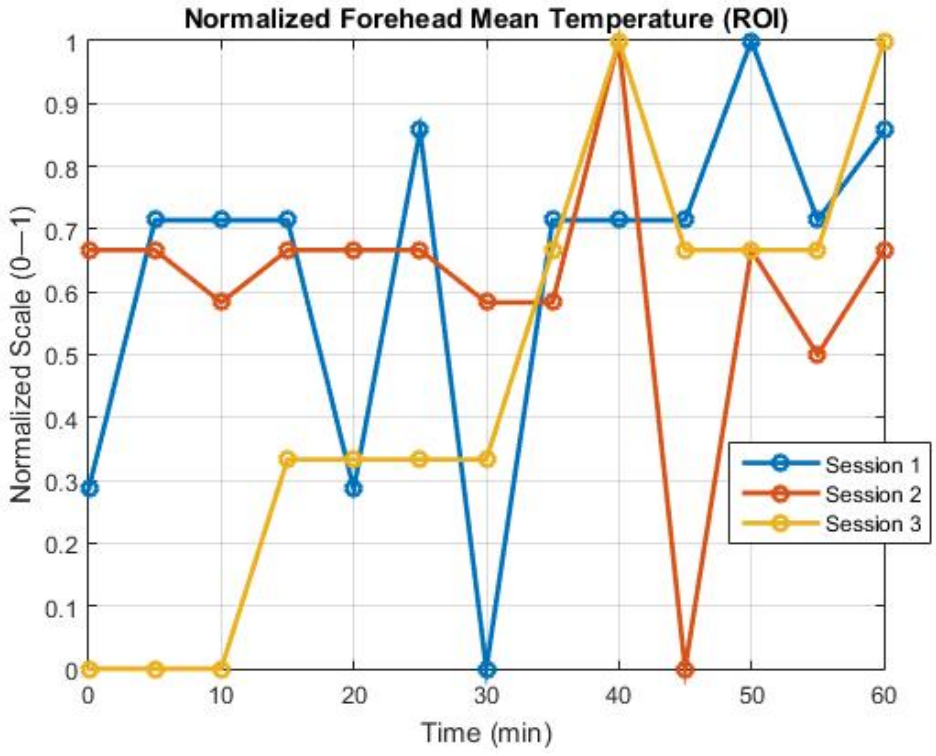


Figure 10. Normalized forehead mean temperature (ROI) for Participant I across three sessions. Normalization (01 scale) enables relative trend comparison independent of absolute temperature offsets. Consistent temporal progression confirms repeatability of thermal behavior across sessions.

Together, these results indicate stable temporal thermal behavior across repeated deployments under comparable driving conditions.

3.7. Temporal Thermal Evolution—Participant II

Figure 11 presents the temporal evolution of thermal metrics for Participant II across three independent driving sessions. The analyzed parameters include center-point temperature, mean forehead temperature within the defined ROI, maximum forehead temperature, and minimum forehead temperature. As in the case of Participant I, the reported time series were generated from single sampled frames extracted at 5 min intervals from the continuous 25 Hz recordings.

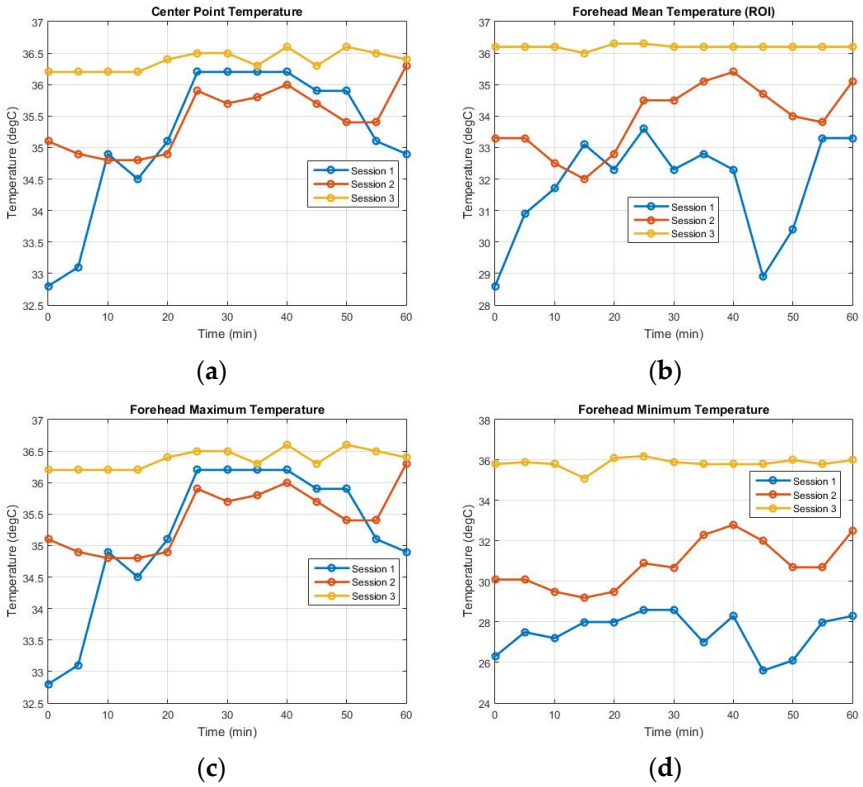


Figure 11. Temporal thermal metrics for Participant II across three independent driving sessions. (**a**) Center-point temperature, (**b**) mean forehead temperature within the ROI, (**c**) maximum forehead temperature, and (**d**) minimum forehead temperature over a 60 min duration. The time series demonstrate stable sensor response and absence of structural drift across sessions.

The center-point temperature (Figure 11a), central point, demonstrates gradual temporal variation without abrupt discontinuities or unstable oscillatory behavior. Although initial temperature levels differ between sessions, the overall progression remains smooth and structurally consistent.

The mean forehead temperature within the ROI (Figure 11b), forehead mean, exhibits a moderate inter-session offset while maintaining coherent trend evolution over time. Session-dependent differences appear primarily as vertical shifts rather than as structural divergence in temporal dynamics. The maximum forehead temperature values (Figure 11c), forehead max, follow patterns consistent with the center-point measurements, indicating stable upper-bound response across sessions.

The minimum forehead temperature values (Figure 11d), forehead min, display greater variability than the mean and maximum metrics. As for Participant I, this behavior is expected because the minimum value is more sensitive to localized cooling, minor posture changes, and transient ROI boundary displacement. After normalization to a 0–1 scale, the

relative temporal dynamics across sessions become more directly comparable, as shown in Figure 12. The normalized trends indicate preserved temporal structure without evidence of progressive instability.

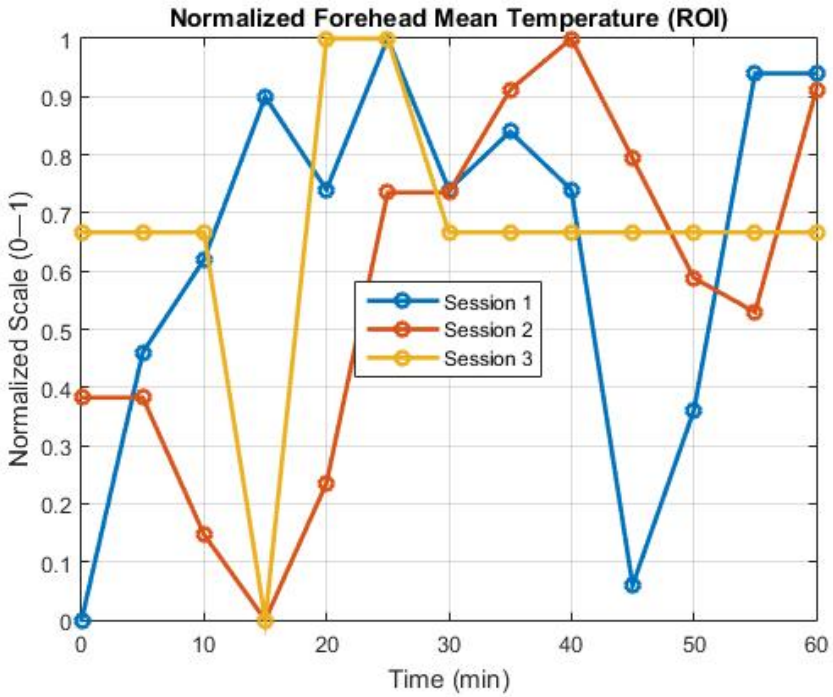


Figure 12. Normalized forehead mean temperature (ROI) for Participant II across three sessions. Normalization (0–1 scale) enables comparison of relative temporal dynamics independent of absolute temperature offsets. The consistent trend structure confirms repeatability of thermal measurements across recording days.

These observations support the repeatable temporal behavior of the LWIR workflow under comparable operating conditions.

The within-session analysis summarized in Table 4 demonstrates low temporal variability across all sessions. The coefficient of variation remained below 5.2% for both participants, indicating stable intra-session thermal behavior. ROI mean temperature slopes ranged from 0.0003 to 0.0365 °C/min, corresponding to gradual and bounded temperature changes over the 60 min recordings. No uncontrolled drift or abrupt instability was observed.

Table 4. Within-session temporal stability metrics.

Participant	Session	ROI Mean Slope (°C/min)	CV (ROI Mean)
P1	S1	0.004	0.006
P1	S2	0.011	0.046
P1	S3	0.005	0.003
P2	S1	0.024	0.052
P2	S2	0.037	0.032
P2	S3	0.000	0.002

The inter-session comparison results are presented in Table 5. Pearson correlation values of mean ROI signals ranged from −0.02 to 0.40, indicating differing absolute temporal patterns across recording days. Root mean square error values ranged between 1.45 °C and 4.67 °C, reflecting baseline temperature offsets rather than structural instability.

Table 5. Inter-session comparison of mean ROI signals.

Participant	Comparison	Pearson r (Mean ROI)	RMSE (°C)
P1	S1 vs. S2	0.107	1.446
P1	S1 vs. S3	0.399	1.999
P1	S2 vs. S3	0.172	2.639
P2	S1 vs. S2	0.098	2.782
P2	S1 vs. S3	−0.021	4.670
P2	S2 vs. S3	0.360	2.493

Within-session stability, as assessed by the coefficient of variation and ROI mean slope (Table 4), indicates that the sampled thermal measurements remained stable within individual sessions. By contrast, the inter-session Pearson correlation values in Table 5 quantify similarity between temporal trajectories recorded on different days and should not be interpreted as direct evidence of sensor stability. The modest correlation values more plausibly reflect day-to-day physiological and contextual baseline variation between sessions.

4. Discussion

The present study evaluated the feasibility, repeatability, and temporal stability of a low-cost long-wave infrared (LWIR) thermal imaging workflow for in-vehicle driver monitoring under real operating conditions. The experimental design incorporated controlled posture validation (Figures 5 and 6), cross-session repeatability analysis (Figures 7 and 8), and sampled time-series thermal evolution across three independent sessions for each participant (Figures 9–12). Taken together, these components provide a multi-layer feasibility framework for assessing whether a consumer-grade mobile LWIR system can preserve sufficient facial thermal consistency for ROI-based monitoring in a real automotive cabin.

4.1. Validation of Camera Position and ROI Stability

Figures 5 and 6 confirm that the selected mounting configuration ensured consistent visibility of the facial ROI across multiple head orientations and posture variations. The comparison between RGB and LWIR images demonstrates that the forehead region remained within the measurement field under the tested pose changes.

The stationary validation condition shown in Figures 5 and 6 reduced motion-related confounding factors and allowed the geometric stability of the measurement setup to be assessed more directly. The preserved thermal contrast across the tested poses indicates that the manually positioned forehead window was not critically dependent on minor head rotations. This supports the geometric suitability of the selected camera placement for feasibility-level facial thermal monitoring inside the vehicle cabin.

4.2. Cross-Session Repeatability

Figures 7 and 8 present representative mid-session thermal frames for both participants across three independent recording days. For both drivers, the facial thermal patterns remained visually coherent, and the maximum displayed temperatures remained within biologically plausible facial ranges. The observed variation between sessions appeared primarily as modest differences in absolute thermal levels rather than as structural distortion of the facial thermal pattern.

Importantly, no persistent hotspot displacement, major contour deformation, or obvious frame-level failure was observed in the representative mid-session images. This supports the interpretation that the app-based LWIR workflow preserved repeatable facial thermal representation across repeated driving sessions performed under comparable environmental conditions.

4.3. Temporal Stability of Thermal Metrics

The time-series results shown in Figures 9–12 provide additional insight into the temporal behavior of the sampled ROI-derived thermal metrics. For both participants, the center-point and mean forehead temperature trajectories remained generally smooth over the 60 min sessions, while maximum values followed similar upper-bound behavior. Minimum values displayed greater fluctuation, which is expected given their higher sensitivity to localized cooling, ROI-edge effects, and minor frame-level placement variation.

For Participant I, an isolated decrease was observed in the mean forehead ROI signal during Session 2. Given the manually assisted ROI workflow, sampled-frame analysis, and app-based temperature interpretation, this event is most appropriately treated as a likely measurement anomaly related to ROI sensitivity or partial peripheral inclusion, rather than as strong evidence of a physiological forehead temperature decrease of such magnitude. This interpretation is consistent with the general stability of the remaining temporal trajectories.

Normalized ROI trends (Figures 10 and 12) further indicate that despite differences in absolute temperature levels between sessions, the relative temporal patterns remained broadly comparable. Within-session stability, as assessed by the ROI mean slope and coefficient of variation (Table 4), supports the conclusion that the sampled thermal measurements remained stable within individual sessions. By contrast, the inter-session Pearson correlation values in Table 5 quantify similarity between trajectories recorded on different days and should not be interpreted as direct evidence of sensor stability. The modest correlations are more plausibly explained by day-to-day physiological and contextual baseline variation, including pre-drive thermal adaptation, clothing insulation, initial physiological state, and small cabin microclimate differences.

4.4. Sensor Performance Under Real Driving Conditions

Unlike laboratory-only validation studies, the present work included real in-vehicle measurements under prolonged driving exposure. The thermal workflow operated under varying head orientations, natural posture adjustments, a realistic cabin environment, and an extended monitoring duration. Despite these uncontrolled micro-variations, the sampled thermal observations remained interpretable and sufficiently stable for manually assisted ROI-based analysis.

Accordingly, the present findings suggest that the examined low-cost LWIR workflow can support feasibility-level facial thermal monitoring under realistic automotive conditions. At the same time, this study does not claim deployable automated driver state classification or full radiometric validation. Rather, it demonstrates that a practical consumer-grade thermal workflow can preserve useful facial thermal consistency for exploratory monitoring applications.

4.5. Scientific Contribution and Novelty

The novelty of the present work lies primarily in its structured validation methodology rather than in the hardware itself. This study contributes a multi-layer feasibility framework combining geometric validation, cross-session repeatability, and temporal consistency assessment for a manually assisted forehead-ROI workflow in a real automotive environment.

Whereas many previous studies have focused on drowsiness classification, algorithmic detection, or multimodal driver state inference, the present work addresses an earlier prerequisite question: whether a compact consumer-grade LWIR workflow can preserve sufficient facial thermal consistency to justify future higher-level driver-monitoring development. In this sense, the contribution of this study is methodological. It does not establish a deployable driver state classifier, but it does provide evidence that a manually

assisted consumer-grade LWIR workflow can support feasibility-level ROI-based thermal monitoring under controlled real driving conditions.

4.6. Limitations

The present study was limited to two healthy adult male participants of similar age. Therefore, the findings cannot be generalized to broader driver populations without further validation across different ages, sexes, facial morphologies, facial hair conditions, eyewear use, health states, and other subject-specific factors that may influence apparent facial thermal patterns.

All sessions were conducted during winter mornings under relatively stable environmental conditions, with outdoor temperatures between approximately −1 °C and 0 °C and a cabin temperature stabilized at approximately 23 °C. These conditions do not represent the full range of in-vehicle thermal environments, such as summer solar loading, rapidly varying cabin thermal fields, or direct HVAC airflow toward the face.

A further limitation is that the forehead temperature window was positioned manually for each selected frame. This manually assisted workflow was intentionally used to avoid losing the target region in low-resolution LWIR imagery, but it is labor-intensive and does not represent a fully automated driver monitoring system. Future work should evaluate the influence of automated face and ROI tracking, including possible boundary jitter and frame-to-frame instability.

In addition, the present workflow did not provide access to raw detector-level radiometric data. Accordingly, the reported temperature-derived values and image stability descriptors should be interpreted as app-based workflow-level measures rather than as strict radiometric calibration metrics or native-sensor noise parameters.

5. Conclusions

This study indicates that the examined low-cost LWIR workflow can provide sufficiently stable, repeatable, and temporally consistent facial thermal observations under realistic in-vehicle conditions.

Geometric validation confirmed that the selected camera placement ensured reliable visibility of the forehead ROI across multiple head orientations and posture changes. Cross-session analysis showed that facial thermal distributions remained structurally consistent without major distortion. Sampled time-series evaluation revealed generally smooth temporal evolution of center-point and ROI-based temperature metrics over 60 min sessions, with no evidence of progressive within-session instability.

Although minor inter-session offsets were observed, normalized analysis confirmed preservation of relative temporal behavior, indicating that the observed variation is more consistent with baseline session offsets than with structural sensor instability. This study therefore supports the feasibility of using a manually assisted consumer-grade LWIR workflow for ROI-based facial thermal monitoring in a real automotive cabin.

The contribution of this work lies in its structured feasibility methodology rather than in hardware innovation. By combining geometric validation, cross-session repeatability, and temporal consistency assessment under realistic driving conditions, this study provides a methodological foundation for future development of thermal-based driver monitoring approaches.

Future research should expand the participant cohort, include more diverse environmental conditions, and integrate automated ROI tracking in order to further evaluate robustness, generalizability, and practical scalability.

Funding: This research was funded by the European Regional Development Fund within the OP "Research, Innovation and Digitalization Programme for Intelligent Transformation 2021–2027", Project No BG16RFPR002-1.014-0005 Center of competence "Smart Mechatronics, Eco- and Energy Saving Systems and Technologies".

Institutional Review Board Statement: This study was conducted according to the guidelines of the Declaration of Helsinki and informed consent was obtained from all the subjects involved in this study. Ethical review and approval were waived for this study due to its retrospective character and the fact that it only involved contactless collected data. This study did not have a medical purpose and therefore does not fall under the jurisdiction of the ethics committee.

Informed Consent Statement: Informed consent was obtained from all subjects involved in the study. Written informed consent for publication of anonymized images was obtained from the participants.

Data Availability Statement: The data presented in this study are available on request from the corresponding author. The datasets consist of thermal image frames recorded during controlled road experiments and processed analysis outputs.

Conflicts of Interest: The author declares no conflict of interest.

Abbreviations

The following abbreviations are used in this manuscript:

ROI	Region of Interest
LWIR	Long-wave Infrared
SIFT	Scale-Invariant Feature Transform
IR	Infrared
RMSE	Root Mean Square Error
AAM	Active Appearance Model
ADAS	Advanced Driver-Assistance System
RGB	Red–Green–Blue

References

1. Choi, I.-H.; Jeong, C.-H.; Kim, Y.-G. Tracking a Driver's Face against Extreme Head Poses and Inference of Drowsiness Using a Hidden Markov Model. *Appl. Sci.* **2016**, *6*, 137. [CrossRef]
2. Birchfield, S. Elliptical head tracking using intensity gradients and color histograms. In Proceedings of the 1998 IEEE Computer Society Conference on Computer Vision and Pattern Recognition (Cat. No. 98CB36231), Santa Barbara, CA, USA, 25 June 1998; pp. 232–237.
3. Basu, S.; Essa, I.; Pentland, A. Motion regularization for model-based head tracking. In Proceedings of the 13th International Conference on Pattern Recognition, Vienna, Austria, 25–29 August 1996; Volume 3, pp. 611–616.
4. Ohayon, S.; Rivlin, E. Robust 3d head tracking using camera pose estimation. In Proceedings of the 18th International Conference on Pattern Recognition (ICPR'06), Hong Kong, China, 20–24 August 2006; Volume 1, pp. 1063–1066.
5. Smith, P.; Shah, M.; da Vitoria Lobo, N. Monitoring head/eye motion for driver alertness with one camera. In Proceedings of the 15th International Conference on Pattern Recognition. ICPR-2000, Barcelona, Spain, 3–7 September 2000; Volume 4, pp. 636–642.
6. Baker, S.; Matthews, I.; Xiao, J.; Gross, R.; Kanade, T.; Ishikawa, T. Real-time non-rigid driver head tracking for driver mental state estimation. In Proceedings of the 11th World Congress on Intelligent Transportation Systems, Beijing, China, 12–15 October 2004.
7. Florez, R.; Palomino-Quispe, F.; Alvarez, A.B.; Coaquira-Castillo, R.J.; Herrera-Levano, J.C. A Real-Time Embedded System for Driver Drowsiness Detection Based on Visual Analysis of the Eyes and Mouth Using Convolutional Neural Network and Mouth Aspect Ratio. *Sensors* **2024**, *24*, 6261. [CrossRef]
8. Hollósi, J.; Ballagi, Á.; Kovács, G.; Fischer, S.; Nagy, V. Bus Driver Head Position Detection Using Capsule Networks under Dynamic Driving Conditions. *Computers* **2024**, *13*, 66. [CrossRef]
9. Kidu, T.; Song, Y.; Seo, K.-W.; Lee, S.; Park, T. An Intelligent Real-Time Driver Activity Recognition System Using Spatio-Temporal Features. *Appl. Sci.* **2024**, *14*, 7985. [CrossRef]
10. Naqvi, R.A.; Arsalan, M.; Batchuluun, G.; Yoon, H.S.; Park, K.R. Deep Learning-Based Gaze Detection System for Automobile Drivers Using a NIR Camera Sensor. *Sensors* **2018**, *18*, 456. [CrossRef] [PubMed]

11. Guo, K.; Zhai, T.; Purushothama, M.H.; Dobre, A.; Meah, S.; Pashollari, E.; Vaish, A.; DeWilde, C.; Islam, M.N. Contactless Vital Sign Monitoring System for In-Vehicle Driver Monitoring Using a Near-Infrared Time-of-Flight Camera. *Appl. Sci.* **2022**, *12*, 4416. [CrossRef]
12. Vijeikis, R.; Dada, I.D.; Abayomi-Alli, A.A.; Raudonis, V. Enhancing Driver Monitoring Systems Based on Novel Multi-Task Fusion Algorithm. *Sensors* **2025**, *25*, 6799. [CrossRef] [PubMed]
13. Zhao, Y.; Görne, L.; Yuen, I.-M.; Cao, D.; Sullman, M.; Auger, D.; Lv, C.; Wang, H.; Matthias, R.; Skrypchuk, L.; et al. An Orientation Sensor-Based Head Tracking System for Driver Behaviour Monitoring. *Sensors* **2017**, *17*, 2692. [CrossRef] [PubMed]
14. Jiménez-Pinto, J.; Torres-Torriti, M. Optical Flow and Driver's Kinematics Analysis for State of Alert Sensing. *Sensors* **2013**, *13*, 4225–4257. [CrossRef] [PubMed]
15. Dong, Y.; Hu, Z.; Uchimura, K.; Murayama, N. Driver inattention monitoring system for intelligent vehicles: A review. *IEEE Trans. Intell. Transp. Syst.* **2010**, *12*, 596–614. [CrossRef]
16. Weiss, C.; Kirmas, A.; Lemcke, S.; Böshagen, S.; Walter, M.; Eckstein, L.; Leonhardt, S. Head Tracking in Automotive Environments for Driver Monitoring Using a Low Resolution Thermal Camera. *Vehicles* **2022**, *4*, 219–233. [CrossRef]
17. Cardone, D.; Perpetuini, D.; Filippini, C.; Mancini, L.; Nocco, S.; Tritto, M.; Rinella, S.; Giacobbe, A.; Fallica, G.; Ricci, F.; et al. Classification of Drivers' Mental Workload Levels: Comparison of Machine Learning Methods Based on ECG and Infrared Thermal Signals. *Sensors* **2022**, *22*, 7300. [CrossRef] [PubMed]
18. Albadawi, Y.; Takruri, M.; Awad, M. A Review of Recent Developments in Driver Drowsiness Detection Systems. *Sensors* **2022**, *22*, 2069. [CrossRef] [PubMed] [PubMed Central]
19. Nordbakke, S.; Sagberg, F. Sleepy at the wheel: Knowledge, symptoms and behaviour among car drivers. *Transp. Res. Part F Traffic Psychol. Behav.* **2007**, *10*, 1–10. [CrossRef]
20. Tayab Khan, M.; Anwar, H.; Ullah, F.; Ur Rehman, A.; Ullah, R.; Iqbal, A.; Lee, B.-H.; Kwak, K.S. Smart real-time video surveillance platform for drowsiness detection based on eyelid closure. *Wirel. Commun. Mob. Comput.* **2019**, *2019*, 2036818. [CrossRef]
21. Tashakori, M.; Nahvi, A.; Shahiidian, A.; Kiashari, S.E.H.; Bakhoda, H. Estimation of driver drowsiness using blood perfusion analysis of facial thermal images in a driving simulator. *J. Sleep Sci.* **2018**, *3*, 45–52.
22. Tashakori, M.; Nahvi, A.; Ebrahimian Hadi Kiashari, S. Driver drowsiness detection using facial thermal imaging in a driving simulator. *Proc. Inst. Mech. Eng. Part H J. Eng. Med.* **2022**, *236*, 43–55. [CrossRef] [PubMed]
23. Bando, S.; Oiwa, K.; Nozawa, A. Evaluation of dynamics of forehead skin temperature under induced drowsiness. *IEEJ Trans. Electr. Electron. Eng.* **2017**, *12*, S104–S109. [CrossRef]
24. Zhou, Z.; Fang, Z.; Wang, J.; Chen, J.; Li, H.; Han, L.; Zhang, Z. Driver vigilance detection based on deep learning with fused thermal image information for public transportation. *Eng. Appl. Artif. Intell.* **2023**, *124*, 106604. [CrossRef]
25. Tan, C.; Wang, H.; Pei, D. SWF-SIFT approach for infrared face recognition. *Tsinghua Sci. Technol.* **2010**, *15*, 357–362. [CrossRef]

Disclaimer/Publisher's Note: The statements, opinions and data contained in all publications are solely those of the individual author(s) and contributor(s) and not of MDPI and/or the editor(s). MDPI and/or the editor(s) disclaim responsibility for any injury to people or property resulting from any ideas, methods, instructions or products referred to in the content.